

1 **Assessing aeolian beach-surface dynamics using a remote sensing**  
2 **approach**

3

4 Irene Delgado-Fernandez<sup>1\*</sup>, Robin Davidson-Arnott<sup>2</sup>, Bernard O.Bauer<sup>3</sup>, Ian J.  
5 Walker<sup>4</sup>, Jeff Ollerhead<sup>5</sup>, Hosahng Rhew<sup>6</sup>

6

7

8 <sup>1</sup>Centre for Coastal & Marine Research, School of Environmental Sciences, University of Ulster,  
9 Coleraine, UK, BT52 1SA

10 <sup>2</sup>Department of Geography, University of Guelph, Guelph, ON, Canada, N1G 2W1,

11 [rdarnott@uoguelph.ca](mailto:rdarnott@uoguelph.ca)

12 <sup>3</sup>Earth & Environmental Sciences and Geography, University of British Columbia, Kelowna, BC,  
13 Canada, V1V 1V7, [bernard.bauer@ubc.ca](mailto:bernard.bauer@ubc.ca)

14 <sup>4</sup>Department of Geography, University of Victoria, Victoria, BC, Canada, V8W 3R4,

15 [ijwalker@uvic.ca](mailto:ijwalker@uvic.ca)

16 <sup>5</sup>Department of Geography & Environment, Mount Allison University, Sackville, NB, Canada,

17 [jollerhead@mta.ca](mailto:jollerhead@mta.ca)

18 <sup>6</sup>Coastal and Estuarine Morphodynamics Laboratory, Department of Oceanography, INHA  
19 University, 253 YongHyun-Dong, Nam-gu, Incheon, 402-751, Korea,

20 [rhew0503@hanmail.net](mailto:rhew0503@hanmail.net)

21

22

23 \*Present address: Natural, Geographical and Applied Sciences, Edge Hill University, St. Helens  
24 Road, Ormskirk, Lancashire, UK, L39 4QP, [delgadoi@edgehill.ac.uk](mailto:delgadoi@edgehill.ac.uk)

25

26 **Abstract**

27 A remote sensing technique for assessing beach surface moisture was used to  
28 provide insight into beach-surface evolution during an aeolian event. An  
29 experiment was carried out on October 21, 2007 at Greenwich Dunes, Prince  
30 Edward Island National Park, Canada, during which cameras were mounted on a  
31 mast on the foredune crest at a height of about 14 m above the beach. Maps of  
32 beach surface moisture were created based on a calibrated relationship between  
33 surface brightness from the photographs and surface moisture content measured  
34 in situ at points spaced every 2.5 metres along a transect using a Delta-T  
35 moisture probe. A time sequence of maps of surface moisture content captured  
36 beach surface evolution through the transport event at a spatial and temporal  
37 resolution that would be difficult to achieve with other sampling techniques such  
38 as impedance probes. Erosion of the foreshore and berm crest resulted in an  
39 increase in surface moisture content in these areas as the wetter underlying  
40 sediments were exposed. Flow expansion downwind of the berm crest led to  
41 sand deposition and a consequent decrease in surface moisture content. Remote  
42 sensing systems such as the one presented here allow observations of the  
43 combined evolution of beach surface moisture, shoreline position, and fetch  
44 distances during short-term experiments and hence provide a comprehensive  
45 rendering of sediment erosion and transport processes.

46

47 **Keywords:** *beach surface moisture, remote sensing, aeolian geomorphology,*  
48 *Greenwich Dunes*

49

## 50 **1. Introduction**

51           Surface moisture is an important control on the threshold of movement for  
52 aeolian transport and likely on the instantaneous transport rate (Belly, 1964;  
53 McKenna Neuman and Nickling, 1989; Namikas and Sherman, 1995; Cornelis  
54 and Gabriels, 2003; Wiggs et al., 2004a; Davidson-Arnott et al., 2008; Nordstrom  
55 et al., 2011). On beaches, surface moisture can be largely variable over time and  
56 space, and it is subject to change during aeolian transport events due to local  
57 erosion that exposes underlying wetter sediments or local accumulation of dry  
58 sand on a previously wetted surface (e.g. Nield et al., 2011). Until recently,  
59 measurements of surface moisture were acquired by taking surface scrapings or  
60 cores, and returning the samples to the laboratory for gravimetric analysis. In  
61 addition to the considerable labour involved and the difficulty of relating the  
62 results to the true moisture content of the surface grain layer itself, this technique  
63 resulted in physical disturbance of the surface through sampling and trampling.  
64 The development of impedance probes such as the Delta-T Theta probe  
65 (Atherton et al., 2001; Wiggs et al., 2004b; Yang and Davidson-Arnott, 2005;  
66 Edwards and Namikas, 2009) allowed more frequent measurements of moisture  
67 content during transport events, but such probes still have the disadvantage that  
68 readings need to be taken at many points and that each measurement integrates  
69 moisture over a sampling depth of about 2-6 cm depending on the length of the  
70 probe.

71           The development of remote sensing technologies for assessing surface  
72 moisture using the apparent surface brightness offers the potential to sample

73 instantaneously over a substantial area without disturbing the surface, and this  
74 approach provides a better measure of the true surface moisture content  
75 (McKenna Neuman and Langston, 2006; Darke et al., 2009; Delgado-Fernandez  
76 et al., 2009). Remote sensing systems have become increasingly important tools  
77 in coastal research, with a number of processes and forms now being monitored  
78 using Argus Systems (Holman and Stanley, 2007), satellite imagery (e.g., Wahid,  
79 2008), Terrestrial Laser Scanner (TLS; Nield and Wiggs, 2011) and time-lapse  
80 photography (e.g., Lynch et al., 2006; Darke et al., 2009; Delgado-Fernandez et  
81 al., 2009). Summerfield (2005, p. 403) notes that it is often the introduction of  
82 new techniques that stimulates 'leaps of explanatory power' and permits  
83 investigation into questions previously discarded as 'incapable of being  
84 addressed'. In particular, the deployment of camera systems for periods of  
85 months to years has provided rich insight into the nature of aeolian transport  
86 events in coastal areas (Delgado-Fernandez and Davidson-Arnott, 2011).

87         The primary purpose of this paper is to discuss the use and potential of a  
88 remote-sensing camera system (Delgado-Fernandez et al., 2009) as part of a  
89 short-term field experiment designed to measure wind flow and sand transport  
90 across a beach foreshore and berm over a period of several hours. In this  
91 application imagery was captured every 5 minutes, in contrast to the hourly data  
92 collected for the meso-scale monitoring (Delgado-Fernandez, 2011). This  
93 allowed detailed assessment of the evolution of surface moisture during the  
94 transport event with the prospect of evaluating the effect of moisture on the  
95 spatial and temporal variations in the sand transport rate. Information derived

96 from the remotely sensed imagery was compared to data from the Theta probe in  
97 order to determine the accuracy and precision of each methodology. The  
98 discussion in this paper focuses on the effects of aeolian transport on surface  
99 moisture content rather than moisture as a control on the threshold of aeolian  
100 transport. While the latter has been widely discussed, the former can now be  
101 investigated by analysing the complexities shown in moisture maps obtained  
102 from the remote sensing system.

103

## 104 **2. Study site**

105 The study site was located at Greenwich Dunes, Prince Edward Island  
106 (PEI), Canada (Figure 1). Greenwich Dunes are part of a barrier spit beach-dune  
107 complex formed on the east side of the entrance to Saint Peter's Bay, on the  
108 north shore of PEI (Mathew et al., 2010). The coast is microtidal with a mixed  
109 semidiurnal regime and a maximum range at spring tides of approximately 1 m.  
110 The foredune ranges in height from 6 to 10 m with a stoss slope of 20-25° and  
111 the dune crest is aligned roughly east-west. The beach is 30-40 m wide and  
112 consists predominantly of quartz sand with a mean diameter of 0.26 mm. Marram  
113 grass (*Ammophila breviligulata*) covers the foredunes and exhibits considerable  
114 seasonal patterns of density and height, with individual plants typically reaching  
115 25 cm heights. The study site was located approximately 1 km east of Saint  
116 Peter's Bay, and covered an area of approximately 60 m alongshore. Further  
117 information on the study site may be found in Hesp et al. (2005), Walker et al.  
118 (2006), Davidson-Arnott et al. (2008) and Bauer et al. (2009).

119 **3. Methods**

120 Wind and sand transport intensity

121 Wind and sand transport were measured using high-frequency  
122 instrumentation deployed at five stations set up at 10 m intervals along a transect  
123 oriented parallel to the wind direction from the top of the foreshore across the  
124 berm crest and upper beach (Figure 2A, B). Wind direction was from the NW at  
125 an angle of about 30° from shore parallel. The foreshore was quite gentle with a  
126 slope of 2° along the transect and a height difference of about 1.2 m between the  
127 berm crest and the low tide terrace (Figure 3B). Station 5 was set up near the  
128 upper foreshore, and station 4 was located on the berm crest. Station 3 was  
129 located on the gently sloping back surface of the berm crest and station 2 was  
130 within a slight dip in the topography that marked the junction between the  
131 landward-dipping berm slope and the seaward dipping beach surface on which  
132 station 1 was located.

133 Wind flow was measured using 2-D and 3-D sonic anemometers deployed  
134 on H-frames at stations 1 to 4 (Figure 2B). Each station consisted of two Gill 3-D  
135 Windmaster sonic anemometers positioned at 0.25 and 1.5 m above the bed,  
136 and a Gill 2-D windsonic anemometer mounted at a height of 3 m. These stations  
137 were positioned at 0, 10, 20 and 30 m along the profile (Figure 3B). An RM  
138 Young cup anemometer was positioned at station 5 near the top of the foreshore  
139 slope (40 m) at a height of 0.25 m. A mast with a vertical array of six cup  
140 anemometers was positioned near the back of the beach, but the data are not  
141 utilised in this paper.

142 Sand transport intensity was measured using two different sensor types:  
143 'Safire' piezoelectric impact sensors (Baas, 2004; Barchyn and Hugenholtz, 2010)  
144 and Wenglor laser sensors (Davidson-Arnott et al., 2009; Hugenholtz and  
145 Barchyn, 2011). The Safires count only grains with sufficient momentum to  
146 register when they strike the 2 cm sensing ring, and grains that are too small, too  
147 slowly moving, or which only graze the sensor are not registered as counts. The  
148 sensitivity of the sensor also varies around the circumference of the instrument,  
149 particularly away from the two 'sweet spots' that mark the point of attachment of  
150 the leads to the sensing ring (Baas, 2004). It has been shown that the sensitivity  
151 varies from one sensor to another, and that sensitivity will vary over time  
152 particularly as the rubber sheathing weathers. The five Safires deployed here  
153 were selected after tests in the laboratory showed that their response to varying  
154 rates of sediment discharge in an air fall column was very similar. The  
155 instruments were deployed with their 'sweet spot' facing directly into the wind,  
156 thus removing concerns of directionality.

157 The laser sensor (Wenglor® model YH03PCT3) consists of a laser and  
158 photo sensor mounted within a U shaped frame with a spacing (path length) of 3  
159 cm and a beam diameter of 0.6 mm. The instrument detects the drop in voltage  
160 at the photo sensor resulting from the passage of individual grains through the  
161 beam. The counting circuitry is contained within the instrument and is capable of  
162 detecting >2000 grains per second. Evaluation of the sensors indicates that they  
163 count all grains (or portions of grains) above the cut-off size that pass through the  
164 beam, irrespective of speed. As with all such sensors, they cannot distinguish

165 between particles entering the beam at exactly the same time so that a few  
166 particles are missed at moderate transport rates. At very large transport rates the  
167 actual count may go down (Hugenholtz and Barchyn, 2011) but this only occurs  
168 during very intense transport events. Transport rates here were never extreme  
169 enough for the latter to be a consideration (Davidson-Arnott et al., 2009).

170 Safires were deployed at all five stations but the sensor at station 4 failed  
171 early in the experiment. Wenglor laser sensors were deployed at stations 2 and 3  
172 and also at a point half way between stations 1 and 2 (identified here as station  
173 1.5). All sensors were sampled at 1 Hz over the course of the experiment.  
174 Because of capacity restrictions the data logger at station 5 had to be  
175 downloaded part way through the experiment resulting in a gap in data collection  
176 from the anemometer and Safire at that station. There was considerable noise in  
177 the data recorded by the anemometer at a height of 0.25 m at station 4 and,  
178 while it was possible to remove some of this through filtering, the uncertainties  
179 introduced into calculations of five-minute means meant that data from this  
180 sensor were discarded. Finally, sand transport rates were measured using  
181 vertical V traps (Nickling and McKenna Neuman, 1997) during four runs with a  
182 duration of 20 minutes (run 1) and 15 minutes (runs 2-4).

183

#### 184 Moisture content and image processing

185 The long-term monitoring station at Greenwich consisted of three digital  
186 SLR cameras operated by a timer that triggered exposures every hour from May  
187 2007 to May, 2010. The cameras were deployed on top of a 6 m mast located on



188 top of the 8 m high foredune crest (Figure 2C). The west camera had a field of  
189 view of approximately 100 m; the north camera covered a field of view of  
190 approximately 40 m alongshore; and the east camera covered an alongshore  
191 distance of 1.5 km. The east camera provided qualitative data on beach and  
192 weather conditions but the west and north cameras were used to extract  
193 numerical information such as moisture maps (MM) or fetch distances (Delgado-  
194 Fernandez et al., 2009). The short-term experiment described in this paper was  
195 conducted over a period of about six hours on October 21, 2007 within the field of  
196 view of the north camera (Figure 3A). Cameras were set to take exposures every  
197 five minutes during the short-term experiment.

198         The camera images were used to obtain time series of a number of key  
199 factors affecting aeolian sediment transport, such as moisture content and fetch  
200 distances (Delgado-Fernandez, 2011). In particular moisture maps (MM) were  
201 created by an automatic process (using Geomatica v9.1-Easi scripts) involving  
202 moisture calibration, image rectification and establishment of spatial extent and  
203 resolution. The process is described in detail by Delgado-Fernandez et al. (2009).

204         Moisture calibration consists of correlating surface brightness recorded by  
205 digital cameras with moisture content measured at the beach surface (Darke et  
206 al., 2009). Digital sampling of pixel brightness was conducted at beach locations  
207 where moisture samples were collected through surface scraping. Pixel  
208 brightness values were normalized against the brightness value of a 'white board'  
209 in order to compensate for the effect of different environmental light in the  
210 exposures due to sun angle and weather conditions. A calibration curve was

211 obtained by plotting normalized brightness against percent moisture content  
212 obtained from laboratory analysis, which allowed subsequent calculation of  
213 moisture values from pixel brightness values (Delgado-Fernandez et al., 2009).  
214 Image rectification transformed oblique imagery into georeferenced data by  
215 matching ground control points deployed within the field of view of the cameras  
216 with their corresponding map coordinates (surveyed with differential global  
217 positioning system). The raster cell size of the output rectified maps was 0.05 m  
218 and was set during the process of image rectification. This was the finest  
219 resolution possible given the area covered by an original pixel located in the  
220 farthest position (relative to the camera) subject to rectification. Shoreline position  
221 was digitized for each MM and vegetation cover was extracted using  
222 unsupervised classifications (Delgado-Fernandez et al., 2009). This allowed  
223 delimiting the beach width, which was used to establish the spatial extent of the  
224 MM.

225         Finally, near-surface moisture content was measured with a Delta-T Theta  
226 probe along the instrument transect at 2.5 m intervals. Sampling points were  
227 marked with rods (Figures 2B and 3) that were visible within the images taken by  
228 the camera. The probe was systematically used on the landward side of the rod,  
229 which allowed subsequent comparison between moisture values obtained with  
230 the Theta-probe and moisture values digitally sampled at the same locations in  
231 the corresponding MM (section 4). Moisture measurements were taken before  
232 runs 1-3 and after run 4 of the trap runs, at approximately 62, 112, 190 and 242  
233 minutes from the start of the experiment. The length of the stainless steel rods of

234 the probe was shortened from the original 6 cm to 2 cm by using a 4 cm thick  
235 dielectric foam (Yang and Davidson-Arnott, 2005).

236

## 237 **4. Results**

### 238 Spatio-temporal variations in wind flow and sediment transport intensity

239 Wind speed averaged over five-minute periods are plotted in Figure 4A  
240 from the start of the experiment at 09:43 until 13:53 (250 minutes later) when  
241 recording ceased for the anemometers at stations 5, 3, 2 and 1. The general  
242 pattern recorded at all four stations was similar, with largest speeds recorded at  
243 station 5 near the top of the foreshore slope. There was an initial increase in  
244 mean speed to about  $8.5 \text{ ms}^{-1}$  at station 5 about 15 minutes after the start of  
245 recording followed by a decrease to about  $7.3 \text{ ms}^{-1}$ . After 60 minutes the speed  
246 increased again, reaching a peak of approximately  $9.5 \text{ ms}^{-1}$  at about 90 minutes,  
247 remaining steady at this speed until 120 minutes and then decreasing to  $8 \text{ ms}^{-1}$   
248 by 160 minutes. The corresponding averages for transport intensity are plotted  
249 for the four safires in Figure 4B and for the three Wenglor laser probes in Figure  
250 4C. The temporal variations in mean sand transport intensity were somewhat  
251 more complex than for winds but showed a similar pattern with a peak early in  
252 the measurement period followed by a period with very low values for transport  
253 intensity and then much larger values between 90 and 120 minutes. This was  
254 followed by decreasing values until the end of the experiment, with the exception  
255 of the Wenglor at station 3, which showed more variability.

256           The spatial pattern of wind speed across the profile can be seen more  
257 clearly by comparing plots of five-minute means for five intervals (Figure 5B) that  
258 are representative of the range of conditions over the recording period, with the  
259 profile along the instrument line (Figure 5A). Except at the very end of the  
260 recording period the wind speed pattern showed largest speeds at station 5 near  
261 the top of the foreshore slope, slightly lower speeds at station 3 near the back of  
262 the berm crest and a further reduction in speed at station 2 located in the shallow  
263 dip of a remnant runnel at the landward end of the berm. Wind speed increased  
264 slightly at station 1 on the back beach. The pattern was consistent with  
265 acceleration due to flow compression as the wind traveled obliquely across the  
266 foreshore slope and then a small deceleration due to flow expansion in the lee of  
267 the berm crest. Unfortunately because of the problems with the lowermost sonic  
268 anemometer at station 4 it was not possible to determine if there was flow  
269 separation, but there is no consistent evidence for this in the records at station 3  
270 and, because of the modest relief and relatively gentle apparent slope of the  
271 oblique transect, it seems likely that flow remained attached over this distance.

272           The largest transport intensity measured by the safires was generally  
273 found at station 3, landward of the berm crest, followed closely by the probe at  
274 station 5 (Figure 5C). Smaller values were recorded at stations 1 and 2; however,  
275 values for transport intensity at station 1 were almost always larger than those for  
276 station 2. The largest values for the Wenglor laser sensors were also recorded at  
277 station 3, with the smallest values recorded at station 2 and somewhat larger  
278 values at the probe located between stations 2 and 1 (station 1.5). This shows

279 that similar spatial patterns of sand transport intensity were recorded by these  
280 two different sensor types.

281 Actual sand transport rates were measured using vertical integrating traps  
282 that were deployed at all five stations. The trap data thus permit some evaluation  
283 of transport conditions at station 4 compared to those at stations 5 and 3 (Figure  
284 5D). Transport rates at station 4 on the berm crest were always larger than at  
285 station 5. This pattern is to be expected if we assume that wind speed was likely  
286 somewhat larger here because of flow acceleration due to flow compression up  
287 the foreshore slope. Transport rates might also be expected to increase across  
288 the profile with increasing fetch and decreasing surface moisture content.  
289 Transport rates at station 4 were also larger than at station 3 except at the very  
290 end of the experiment when wind speed had decreased considerably. At this time  
291 it would be expected that the combination of light winds and large surface moisture  
292 on the foreshore slope would result in conditions that were below the threshold  
293 for much of the time at this location, and transport would be largely confined to  
294 entrainment of dry sand from the surface of the berm and backshore.

295

#### 296 Spatio-temporal variations in surface moisture

297 Images of the beach were acquired every five minutes, which resulted in a  
298 total of 50 MM. An examination of the moisture conditions at this frequency  
299 revealed that changes were difficult to discern, and hence, 30-minute time  
300 intervals were used to assess changes in surface moisture (Figure 6A). A  
301 representative sample corresponding to the middle period of the experiment is

302 shown here, from approximately 10:30 (55 min) to 13:00 (205 min). In addition to  
303 the moisture maps themselves, difference maps were generated by subtracting  
304 the data for each raster in one time period from the data for the same raster in  
305 the previous time period (Figure 6B). Three classes of surface moisture change  
306 were utilised: no change, drier, and wetter, with the last two classes  
307 corresponding to a decrease or increase in moisture content  $> 2\%$  respectively.  
308 The surface at the end of the first hour was slightly damp, ranging from 2 to 6%  
309 moisture content. A gradual increase in near-surface wind speed from 50 to 100  
310 minutes (Figure 4A) led to erosion of a surficial layer of dry sand from the  
311 foreshore resulting in the west area beach surface becoming wetter at 85  
312 minutes (Figure 6A). Wind speed continued to increase up to 115 minutes and  
313 remained steady and relatively strong until approximately 125 minutes. MM from  
314 85 minutes to 145 minutes show a surface that progressively became drier on the  
315 backshore (due to deposition of dry sand) but especially wetter on the foreshore  
316 and west area (due to progressive erosion), as shown in the maps of changes in  
317 moisture content (Figure 6B). In contrast with the first part of the experiment, the  
318 foreshore became gradually dryer at 175 and especially at 205 minutes, with the  
319 formation of a continuous patch of dry sediment in front of all stations. This was  
320 due to a combination of sunnier conditions favouring evaporation across the  
321 beach surface and relatively gentle winds not capable of eroding the newly dried  
322 sand in the foreshore.

323         Moisture measurements with the Theta probe (Fig 7B) showed relatively  
324 small moisture content (5-7%) across the backshore, increasing moisture at the

325 berm and upper foreshore (6-8%), and the largest moisture content on the lower  
326 foreshore (9-12%). Moisture content was also re-sampled using the digital MM  
327 for the same locations at two grid resolutions: 0.05 m (Figure 7C) and 0.5 m  
328 (Figure 7D). The latter were created through a process of image coarsening,  
329 which combines cells into a larger cell and averages the values of the cells  
330 contained within it (Woodcock and Strahler, 1987). In the example used here,  
331 each 0.5 m cell represents the average of 100 0.05 m cells. The trends obtained  
332 from the MM followed, in general terms, those identified with the Theta probe.  
333 However the readings obtained from the coarser resolution maps (Figure 7D)  
334 showed simpler trend patterns, while moisture values sampled from the finest  
335 resolution maps (Figure 7C) showed unrealistically large variability. Average  
336 values from the 0.5 m renditions were therefore adopted for the purpose of  
337 comparison to the Theta probe values. Figure 8 shows a comparison of moisture  
338 content values obtained from the Theta probe along the profile versus those  
339 obtained from MM at 0.5 m grid resolution for different time intervals. In general,  
340 moisture values obtained from MM presented larger variability, with both drier  
341 and wetter zones than those obtained from the Theta probe. The remote sensing  
342 images seem highly sensitive to slight wetting or drying of the surface while this  
343 does not show up in the Theta probe results. Note that moisture readings taken  
344 close to the east side of the image (e.g., 15 m) at 112 minutes were greater than  
345 what would be expected from a dry surface. These are currently being explored  
346 as they could be a product of inaccuracies of moisture values at the edges of the

347 MM or a product of slight drizzle earlier in the morning, since they are no longer  
348 visible later in the day (see following section).

349

### 350 Co-evolution of surface moisture and sediment transport

351 Figure 9 shows time series for wind direction, wind speed, fetch distance,  
352 moisture content obtained from the 0.5 m grid resolution MM, and transport  
353 intensity given by the Safires for stations 1-5. Wind direction and speed data are  
354 from the 2-D sonic at a height of 3 m at station 4 and are used to provide general  
355 information of the incident wind field since this should be unaffected by growth of  
356 the boundary layer associated with compression of flow up the foreshore slope.  
357 Gaps in the moisture and fetch graphs correspond to periods of time when no  
358 images were taken. Wind direction was initially very constant, from approximately  
359 10° to the E of the instrument transect (aligned with a wind direction of 180°),  
360 gradually becoming more onshore (where directly onshore is 270°) and staying at  
361 20° to the E of the instrument transect by the end of the experiment. Figure 3C  
362 shows the approximate location of the shoreline at the beginning and end of the  
363 experiment, with small changes at this particular location. However, the  
364 combined effect of a rising tide and gradual change in wind direction resulted in a  
365 decrease of available fetch distance towards the end of the experiment,  
366 especially in the landward stations because of differences in beach configuration  
367 (see DEM of Figure 3A). The fetch distance decreased over the course of the  
368 experiment by 9 m at station 5 and 22 m at station 1 (Figure 9). This reduced  
369 fetch has significant implications for sediment transport potential across the



370 beach and may explain, in part, why transport intensity after about 140 minutes  
371 was greatly reduced (Fig 9E).

372         The beginning of the experiment was marked by cloudy conditions and  
373 occasionally light drizzle, which when combined with relatively calm wind  
374 conditions may have played a role in the reduction in sand transport during the  
375 first hour. The drizzle ended about 50 minutes into the experiment, and soon  
376 after that the clouds cleared so that evaporation due to solar radiation became a  
377 factor in the reduction of surface moisture content during the latter half of the  
378 experiment. Increased sediment transport during the second hour likely reflects  
379 both increasing wind speed and surface evaporation. Note that while this is the  
380 trend at stations 4 and 3 (Figure 9D), station 5 (closer to the foreshore) was  
381 characterised by increasing surface moisture content due to progressive stripping  
382 of the dry surface sediment and exposure of the wetter materials below.

383         The foreshore and lower beach were erosion zones whereas the back  
384 beach was a deposition zone. At the end of the transport event, measurements  
385 showed that about 5 cm of scour had occurred at station 5 with a smaller amount  
386 at station 4 on the berm crest (Figure 10A). In contrast about 5 cm of deposition  
387 was measured at station 3, 3 cm at station 2, and about 1 cm at station 1 (Figure  
388 10B). The configuration of this spatial zonation from shoreline to the foredune toe  
389 became gradually aligned normal to the incoming wind direction as the event  
390 progressed, with a transition zone in between strongly affected by beach  
391 topography and shoreline position. The transition zone was a relatively wide area  
392 (roughly around station 4) with a mixture of moist and dry conditions, and

393 characterized by a fairly corrugated edge line resulting from transport processes  
394 acting on a very complex surface due to the presence of stones, flotsam, and  
395 footprints characterising the erosional surface (Figures 6 and 10C). This level of  
396 complexity favours spatial approaches such as MM and remotely sensed data  
397 over spot measurements along single transects such as those collected from  
398 Theta-T probes, which do not provide enough detail on spatial textures.

399

## 400 **5. Discussion**

401 Comparison of Theta-T and MM moisture values raise a number of  
402 questions regarding the assessment of surface moisture content as a primary  
403 control on aeolian sediment transport. Values from MM of 0.5 m resolution  
404 showed a better correlation with the Theta-T probe values, which are reliable  
405 indicators of surface moisture content when there are smooth transitions in  
406 moisture gradients along a given beach transect. Values from MM at 0.05 m  
407 resolution contain a large degree of variability in moisture readings, and the  
408 question is whether such variation is 'noise' or a true representation of the nature  
409 of the evolving beach surface during a transport event. When transport was  
410 active, there were discrete zones of dry sand that were being deposited beside a  
411 moist transport surface that was recently eroded. For example, Figure 2B shows  
412 a complex surface with moisture patches alongside dry sand as a result of active  
413 aeolian streamers and deposition/erosion processes. In this instance, the MM  
414 appear to be yielding 'noisy' but detailed information that may be representative  
415 of the complex evolution of the beach surface through time. Further analysis is

416 being undertaken to investigate these micro-scale complexities and to assess the  
417 accuracy of moisture data at the edges of MM.

418 A related issue has to do with quantifying a characteristic moisture value  
419 that should be used in explanations of sediment transport as a function of wind,  
420 moisture, and fetch distances. The 0.05 m resolution MM provide detailed  
421 representations of beach surface moisture but sediment transport rates might  
422 correlate better with averaged moisture values over a given area. Furthermore,  
423 transport rates could be better explained using some measure of the spatial  
424 distribution of moisture values over a set distance (e.g., 1 m, 2 m, or 10 m) in  
425 front of a given trap. MM provide an excellent platform for these types of  
426 investigations because they allow analysis of moisture content at different spatial  
427 resolutions.

428 In addition to providing a measure of the actual moisture content of the  
429 upper-most sand grain layer, in contrast to the depth-averaged sample (from 1.5-  
430 6 cm thickness) from the Theta probe (Atherton et al., 2001; Yang and Davidson-  
431 Arnott, 2005; Schmutz and Namikas, 2011), the process of cell aggregation of  
432 fine resolution (0.05 m) MM into coarser resolution (0.5 m) MM offers the  
433 advantage of providing more representative spatially-average values. Detailed  
434 sampling of surfaces with moderate moisture content using the Theta probe have  
435 shown that there can be a large degree of variability within an area as small as 1  
436 m<sup>2</sup> (Yang and Davidson-Arnott, 2005; Edwards and Namikas, 2009). While Theta  
437 probes provide point measurements that are assumed to be representative of a  
438 given area, a cell from the coarse resolution MM presented here would represent

439 the average of 100 moisture measurements over an area of 0.5 m<sup>2</sup>. Taking a  
440 similar size sample with a Theta probe would be intrusive and obviously highly  
441 time consuming.

442 While surface moisture is an important control on aeolian transport (Belly,  
443 1964; McKenna Neuman and Nickling, 1989; Namikas and Sherman, 1995;  
444 Cornelis and Gabriels, 2003; Wiggs et al., 2004b; Davidson-Arnott et al., 2008)  
445 results from this study demonstrate that transport is in turn an important control  
446 on surface moisture content as the beach surface evolves through localized  
447 erosion and deposition. Surface moisture is related to transport in two opposing  
448 ways. Safires at stations 5 (foreshore) and 3 (back beach) recorded a peak of  
449 transport intensity from approximately 80 to 120 minutes, coinciding with the  
450 increase of wind speed. However, surficial moisture content increased at station  
451 5 but decreased at station 3 (Figure 9). The combination of flow acceleration up  
452 the foreshore slope and a short fetch (no sediment source upwind) transformed  
453 the foreshore (station 5) into an erosive zone. Hence, relatively large values for  
454 moisture content at this location were the result of sediment erosion and  
455 landward transport. This is in line with observations on sediment transport  
456 dynamics on a drying beach by Nield et al. (2011) who reported erosion of dry  
457 sediment leading to an increase of surface moisture due to the exposure of the  
458 underlying, wetter surface. Large transport rates at station 3 (back beach) were  
459 associated with significant accumulation of dry sand and hence small values of  
460 surface moisture content. Details of the temporal evolution of moisture content in  
461 these two different zones reveal complex feedbacks between moisture, wind

462 speed, sand transport, and fetch distances where moisture is not only a control  
463 for sediment movement but also a result of patterns of erosion and accumulation.  
464 The largest transport rates at stations 5 and 3 were recorded during the first trap  
465 run (96 minutes; Figure 5D), coinciding with the strongest wind speeds and the  
466 peak of saltation recorded by the Safires (Figure 9). As suggested by the MM  
467 (Figure 6A) most of the sand collected during this run at station 5 was the result  
468 of the erosion of a relatively dry layer from the foreshore, which in turn increased  
469 the surface moisture content there. Transport rates at station 5 during the second  
470 run (127 minutes) were smaller than at station 1 (Figure 5D) despite strong winds  
471 of  $9\text{-}9.5\text{ ms}^{-1}$  similar to those recorded during run 1. Hence the erosion of the  
472 layer of dry sediment from this zone during run 1 produced larger levels of  
473 surface moisture during run 2, which in turn limited further erosion. At stations 3-  
474 1, dry sediment stripped from the foreshore was deposited progressively leading  
475 to drier surface sediment. These deposits are easily mobilized under stronger  
476 wind conditions, but boundary layer evolution leads to reduced surface shear  
477 stress and hence, deposition toward the toe of the dune.

478

## 479 **6. Conclusion**

480 This paper demonstrates the applicability of a remote sensing system to  
481 measuring beach surface moisture over a short-term experiment. The detailed  
482 temporal and spatial resolution of the evolution of surface moisture provided by  
483 the time-lapse photography provides an improved explanation for the spatial and  
484 temporal patterns of sand transport, and the changes in the beach surface

485 resulting from scour and deposition. The conclusions can be summarised as  
486 follows:

487 1) Spatial patterns of erosion, transport and deposition over the foreshore  
488 and berm reflect the changing boundary layer produced by flow  
489 compression up the foreshore slope and then expansion over the reverse  
490 slope on the landward side of the berm;

491 2) Temporal patterns of sand transport intensity reflect both changes in wind  
492 speed and direction (fetch distance) over the event, upwind sources of  
493 available dry sediment, and the effects of changes in surface moisture;

494 3) Fine resolution moisture maps offer the possibility of data aggregation  
495 through pixel coarsening and may be used to explore appropriate moisture  
496 values for different applications. While averaged moisture values obtained  
497 from coarser resolution (0.5 m) MM were more similar to those obtained  
498 with the Theta probe these may be smoothing out important micro-scale  
499 information. Further research should be conducted to determine the  
500 appropriate temporal and spatial resolution of moisture measurements.

501 4) The high resolution of the surface MM permits the identification of changes  
502 in moisture over the whole surface that reflect external conditions such as  
503 solar radiation input and precipitation as well as internal conditions  
504 produced by the erosion (wetting) and deposition (drying) of sand.

505 5) The remote sensing system thus provides a relatively simple approach to  
506 measuring the evolution of the beach surface during a transport event, and

507 to providing more comprehensive explanations of processes of erosion  
508 and transport and changes in surface conditions.

509

## 510 **Acknowledgements**

511 We thank Parks Canada for granting permission to carry out work at Greenwich  
512 Dunes and personnel at Greenwich Dunes for their support in the field, especially  
513 Kirby Tulk, Allan Doyle, Tarah McFee, Roger Steadman, and Miguel Santos.  
514 Rosie Smith conducted the DGPS surveys, Mario Finoro and Sandy McLean  
515 provided technical support with building and testing equipment, and Adam  
516 Bonnycastle aided in the development of scripts. Financial support was provided  
517 through a Natural Sciences and Engineering Research Council of Canada  
518 Discovery Grant to RD-A, through a research grant from Parks Canada to RD-A,  
519 IJW and JO, and through the Ontario Graduate Scholarship Program and  
520 University of Guelph Lattornell Travel grant to ID-F.

521

## 522 **References**

523 Atherton R.J, Baird, AJ, Wiggs GFS. 2001. Inter-tidal dynamics of surface  
524 moisture content on a meso-tidal beach. *Journal of Coastal Research* **17** :  
525 482-489.

526 Baas AC W. 2004. Evaluation of saltation flux impact responders (Safires) for  
527 measuring instantaneous aeolian sand transport intensity. *Geomorphology*  
528 **59** : 99-118.

529 Barchyn TE, Hugenholtz CH. 2010. Field comparison of four piezoelectric  
530 sensors for detecting aeolian sediment transport. *Geomorphology* **120** :  
531 368-371.

532 Bauer BO, Davidson-Arnott RGD, Hesp PA, Namikas SL, Ollerhead J, Walker IJ.  
533 2009. Aeolian sediment transport on a beach: surface moisture, wind fetch,  
534 and mean transport. *Geomorphology* **105** : 106–116.

535 Belly PY. 1964. Sand movement by wind. U.S. Army Corps of Engineers CERC,  
536 Tech. Memo. 1 : 38 pp.

537 Cornelis WM, Gabriels D. 2003. The effect of surface moisture on the  
538 entrainment of dune sand by wind: an evaluation of selected models.  
539 *Sedimentology* **50** : 771-790.

540 Darke I, Davidson-Arnott RGD, Ollerhead J. 2009. Measurement of Beach  
541 Surface Moisture Using Surface Brightness. *Journal of Coastal Research*  
542 **26** : 248-256.

543 Davidson-Arnott RGD, Yang Y, Ollerhead J, Hesp PA, Walker IJ. 2008. The  
544 effects of surface moisture on aeolian sediment transport threshold and  
545 mass flux on a beach. *Earth Surface Processes and Landforms* **33** : 55–74.

546 Davidson-Arnott RGD, Bauer BO, Walker IJ, Hesp PA, Ollerhead J, Delgado-  
547 Fernández I. 2009. Instantaneous and mean aeolian sediment transport  
548 rate on beaches: an intercomparison of measurements from several  
549 sensor types. *Journal of Coastal Research*, SI 56, 297-301.



550 Delgado-Fernandez I, Davidson-Arnott RGD, Ollerhead J. 2009. Application of a  
551 remote sensing technique to the study of coastal dunes. *Journal of*  
552 *Coastal Research* **25** : 1160–1167.

553 Delgado-Fernandez I. 2011. Meso-scale modelling of aeolian sediment input to  
554 coastal dunes. *Geomorphology* **130** : 230-243.

555 Delgado-Fernandez I, Davidson-Arnott RGD. 2011. Meso-scale aeolian sediment  
556 input to coastal dunes: The nature of Aeolian transport events.  
557 *Geomorphology* **126** : 217–232

558 Edwards BL, Namikas SL. 2009. Small-scale variability in surface moisture on a  
559 fine-grained beach: implications for modeling aeolian transport. *Earth*  
560 *Surface Processes and Landforms* **34** : 1333-1338.

561 Hesp PA, Davidson-Arnott RGD, Walker IJ, Ollerhead J. 2005. Flow dynamics  
562 over a foredune at Prince Edward Island, Canada. *Geomorphology* **65** :  
563 71-84.

564 Holman RA, Stanley J. 2007. The history and technical capabilities of Argus.  
565 *Coastal Engineering Research Centre* **54** : 477-491.

566 Hugenholtz CH, Barchyn TE. 2011. Laboratory and field performance of a laser  
567 particle counter for measuring aeolian sand transport. *Journal of*  
568 *Geophysical Research*. **116** : F01010, 13 pp. doi:10.1029/2010JF001822

569 Lynch K, Jackson DWT, Cooper AG. 2006. A remote-sensing technique for the  
570 identification of aeolian fetch distance. *Sedimentology* **53** : 1381-1390.

571 Mathew S, Davidson-Arnott RGD, Ollerhead J. 2010. Evolution of a beach–dune  
572 system following a catastrophic storm overwash event: Greenwich Dunes,

573 Prince Edward Island, 1936–2005. *Canadian Journal of Earth Science*. **47**  
574 : 1–18

575 McKenna Neuman C, Nickling WG. 1989. A theoretical and wind tunnel  
576 investigation of the effects of capillary water on the entrainment of  
577 sediment by wind. *Canadian Journal of Soil Science* **69** : 79-96.

578 McKenna Neuman C, Langston G. 2006. Measurement of water content as a  
579 control of particle entrainment by wind. *Earth Surface Processes and*  
580 *Landforms* **31** : 303–317.

581 Namikas SL, Sherman DJ. 1995. A review of the effects of surface moisture  
582 content on aeolian sand transport. *Desert Aeolian Processes*. V. P.  
583 Tchakerian. London, Chapman and Hall Ltd : 269-293.

584 Nickling WG, McKenna Neuman C. 1997. Wind tunnel evaluation of a wedge-  
585 shaped aeolian transport trap. *Geomorphology* **18** : 333-345.

586 Nield JM, Wiggs GFS. 2011. The application of terrestrial laser scanning to  
587 aeolian saltation cloud measurement and its response to changing surface  
588 moisture. *Earth Surface Processes and Landforms* **36** : 273–278.

589 Nield JM, Wiggs GFS, Squirrell RS. 2011. Aeolian sand strip mobility and  
590 protodune development on a drying beach: examining surface moisture  
591 and surface roughness patterns measured by terrestrial laser scanning.  
592 *Earth Surface Processes and Landforms* **36** : 513–522.

593 Nordstrom KF, Jackson NL, Korotky KH, Puleo JA. 2011. Aeolian transport rates  
594 across raked and unraked beaches on a developed coast. *Earth Surface*  
595 *Processes and Landforms* **36** : 779–789.

596 Schmutz PP, Namikas SL. 2011. Utility of Delta-T Theta probe for obtaining  
597 surface moisture measurements from beaches. *Journal of Coastal*  
598 *Research* **27** : 478-484.

599 Summerfield MA. 2005. The changing landscape of geomorphology. *Earth*  
600 *Surface Processes and Landforms* **30** : 779-81.

601 Wahid AM. 2008. GIS-Based Modeling of Wind-Transported Sand on the Qaa  
602 Plain Beach .Southwestern Sinai. Egypt. *Journal of Coastal Research* **24** :  
603 936-943.

604 Walker IJ, Hesp PA, Davidson-Arnott RGD, Ollerhead J. 2006. Topographic  
605 Steering of Alongshore Airflow over a Vegetated Foredune: Greenwich  
606 Dunes, Prince Edward Island, Canada. *Journal of Coastal Research* **22** :  
607 1278-1291.

608 Wiggs GFS, Baird AJ, Atherton RJ. 2004a. The dynamic effects of moisture on  
609 the entrainment and transport of sand by wind. *Geomorphology* **59** : 13–30.

610 Wiggs GFS, Atherton RJ, Baird AJ. 2004b. Thresholds of aeolian sand transport:  
611 establishing suitable values. *Sedimentology* **51** : 95–108.

612 Woodcock CE, Strahler AH. 1987. The factor of scale in remote sensing. *Remote*  
613 *Sensing of Environment* **21** : 311-332.

614 Yang Y, Davidson-Arnott RGD. 2005. Rapid measurement of surface moisture  
615 content on a beach. *Journal of Coastal Research* **21** : 447–452.

616

617

618

619 **List of Figures**

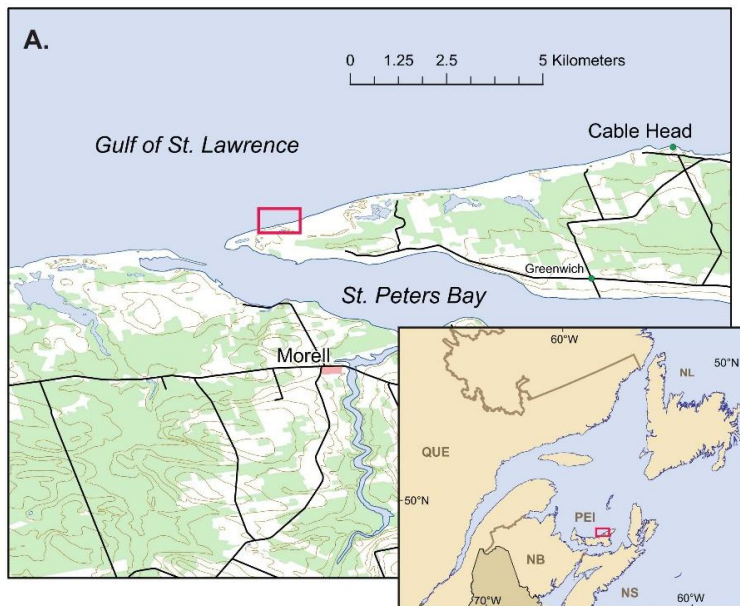


Figure 1: Location of study site at Greenwich Dunes, Prince Edward Island (Canada).

620

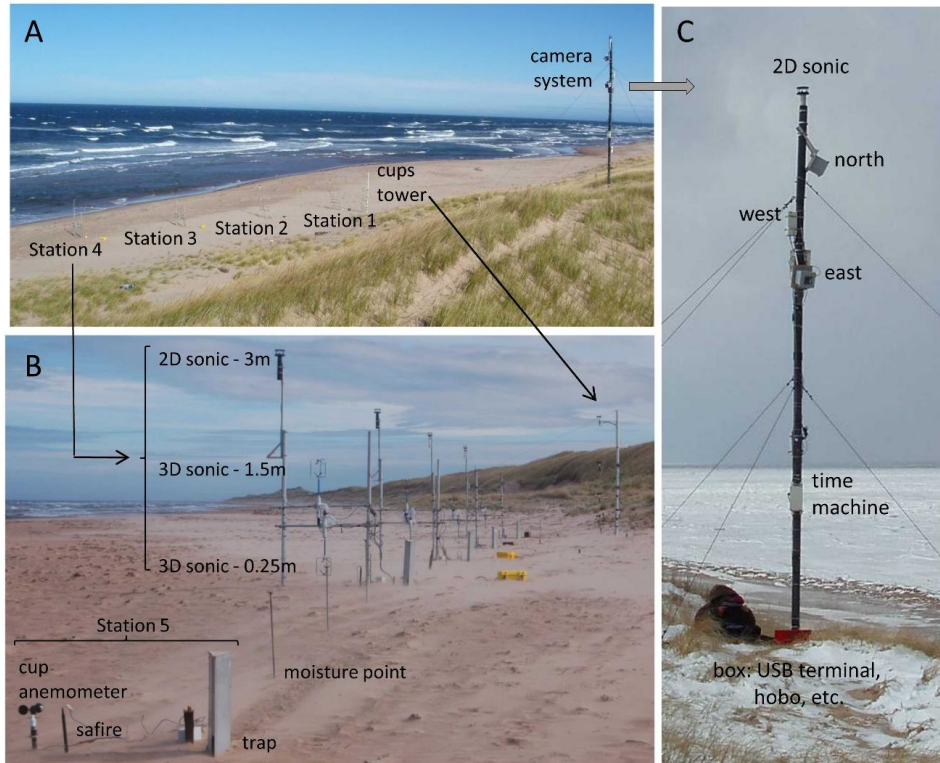


Figure 2: A) General view of study site and instruments; B) close-up of instruments setup. The transect consisted of four stations, each with one 2D and two 3D sonic anemometers located at 3, 1.5, and 0.25 m over the beach surface, and one station with a cup anemometer at 0.25 m over the beach surface. Traps and safires were co-located at each of the stations and moisture points selected every 2.5 m. The transect ran into the incoming wind direction (oblique onshore) and ended in a tower of cup anemometers close to station 1; C) close-up of camera system.

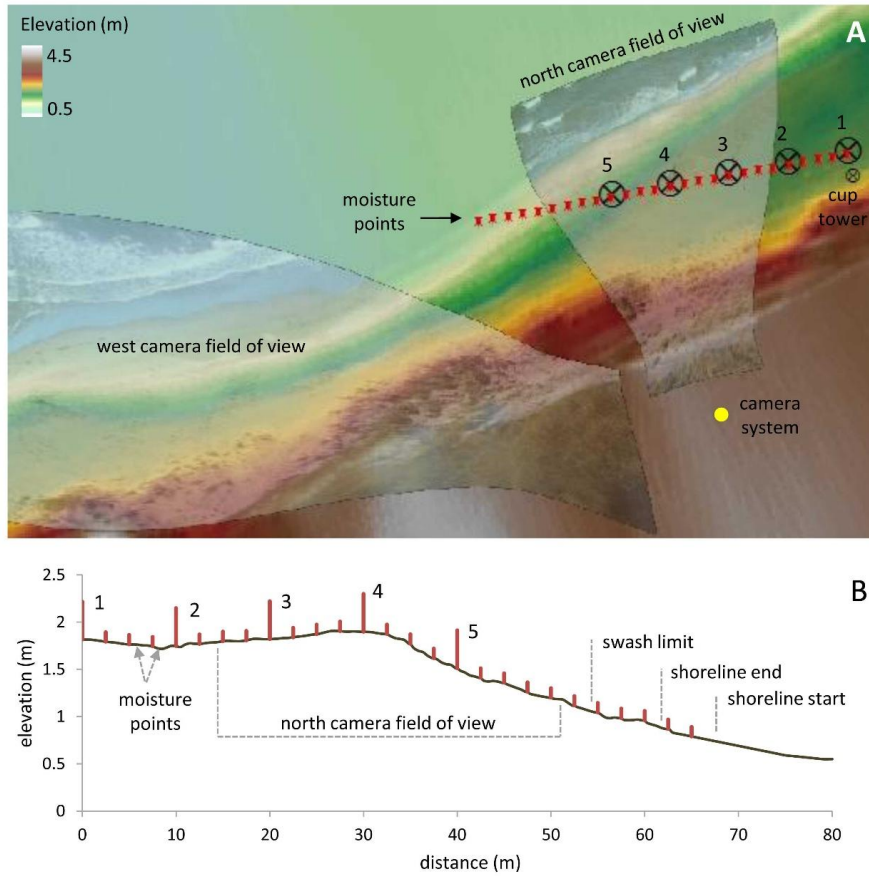


Figure 3: A) Digital elevation model (DEM) georectified from 1 m spot resolution differential global positioning system (DGPS) data. Topographic data was gathered on the beach surface and up to the dune toe and thus the DEM does not include the dune. The position of each station is marked with the station number. Stations 3-5 and a total of 15 moisture points were within the north camera field of view (inserted as a semi-transparent image); B) topographic profile along the instruments transect, showing the approximate location of the shoreline position at the beginning (shoreline start) and end of the experiment.

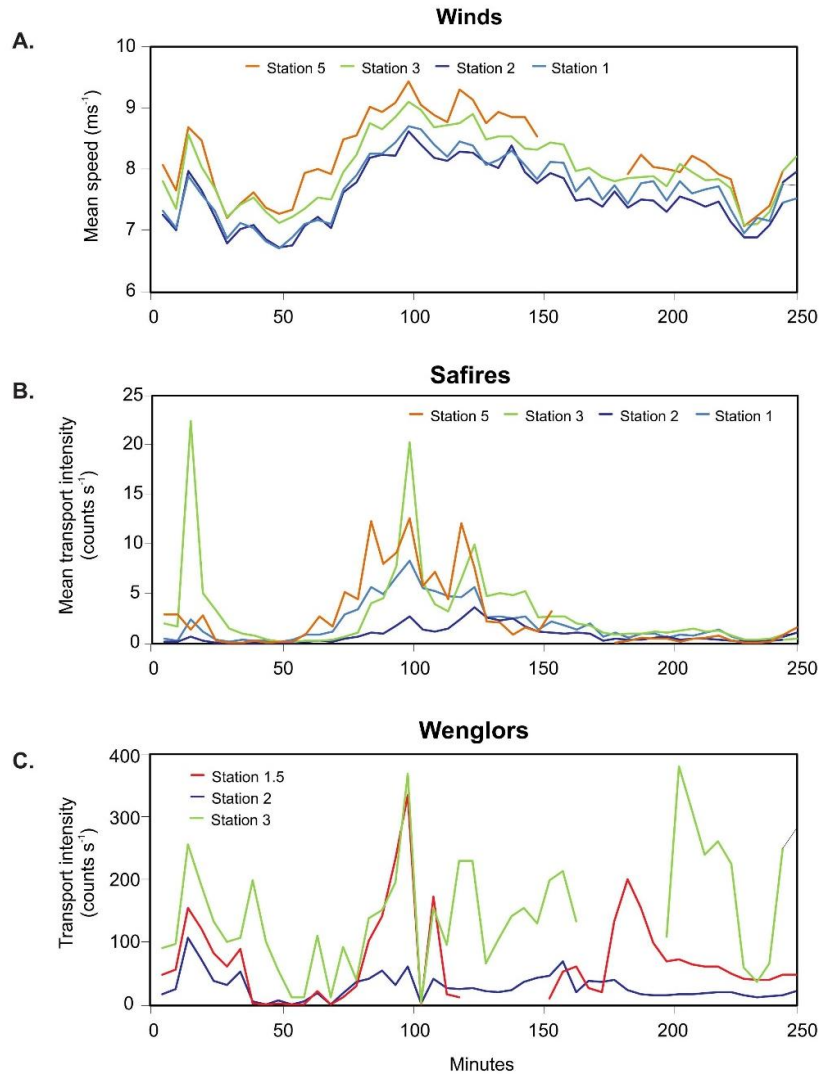


Figure 4: Temporal variations in wind speed and sediment transport intensity. A) five-minute averages for wind speed ( $\text{ms}^{-1}$ ) measured at stations 1, 2, 3 and 5 at 0.25 m height; B) average saltation intensity ( $\text{counts s}^{-1}$ ) measured by Safire probes at the same stations; C) average saltation intensity ( $\text{counts s}^{-1}$ ) measured by Wenglor laser sensors at stations 2, 3 and midway between 1 and 2. Note that the grain counts measured by the Wenglors are much larger than those measured by the Safires (see Davidson-Arnott et al., 2009).

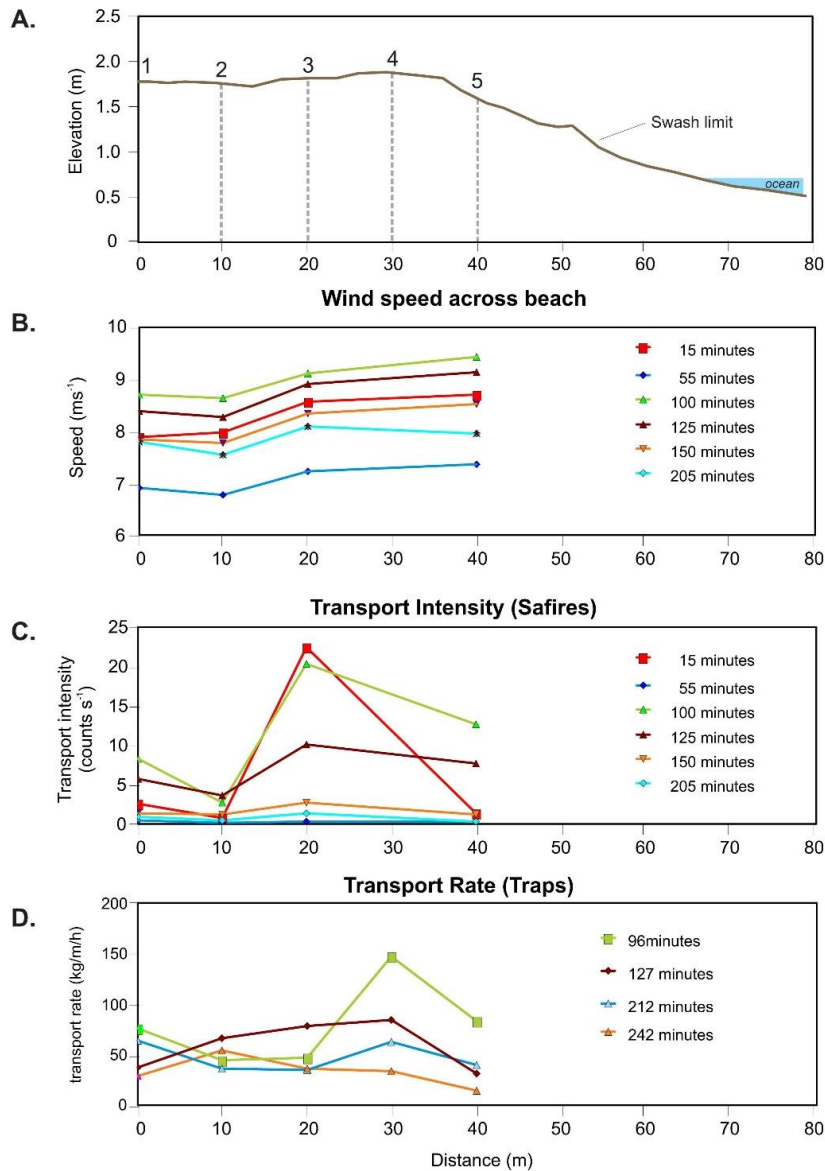


Figure 5: Spatial pattern of winds and sediment transport. A) beach profile along instruments transect; B) mean wind speeds for 6 five minute periods; C) transport intensity measured by the Safire probes for the same 5 minute periods as B); D) transport rate measured by vertical traps. Run 1 had a duration of 20 minutes and the other three runs a duration of 15 minutes. Times are for the end of the run.



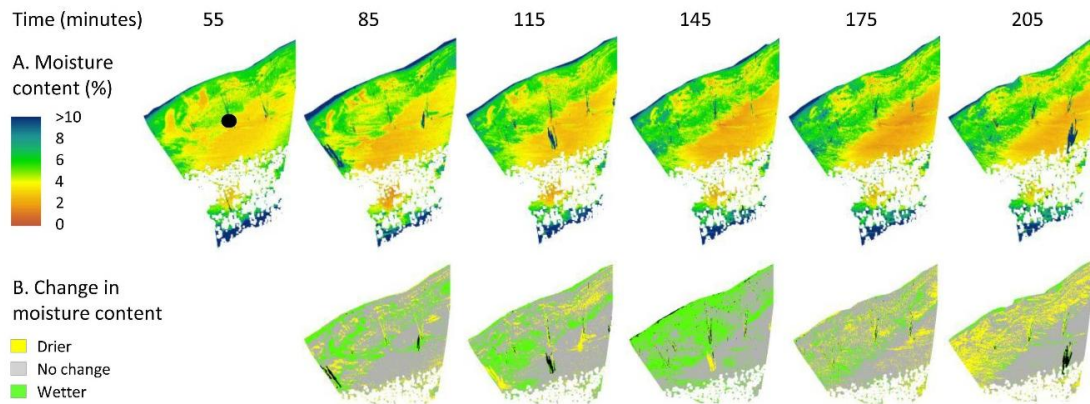


Figure 6: Temporal variations in moisture content. A) temporal sequence of moisture maps every 30 minutes; B) maps showing the change in moisture content relative to the previous moisture map. Only relative changes over  $\pm 2\%$  have been considered, with drier areas (change  $> 2\%$ ) shown in orange and wetter areas (changes  $> -2\%$ ) in green. The black dot shows the location of station 4.

625

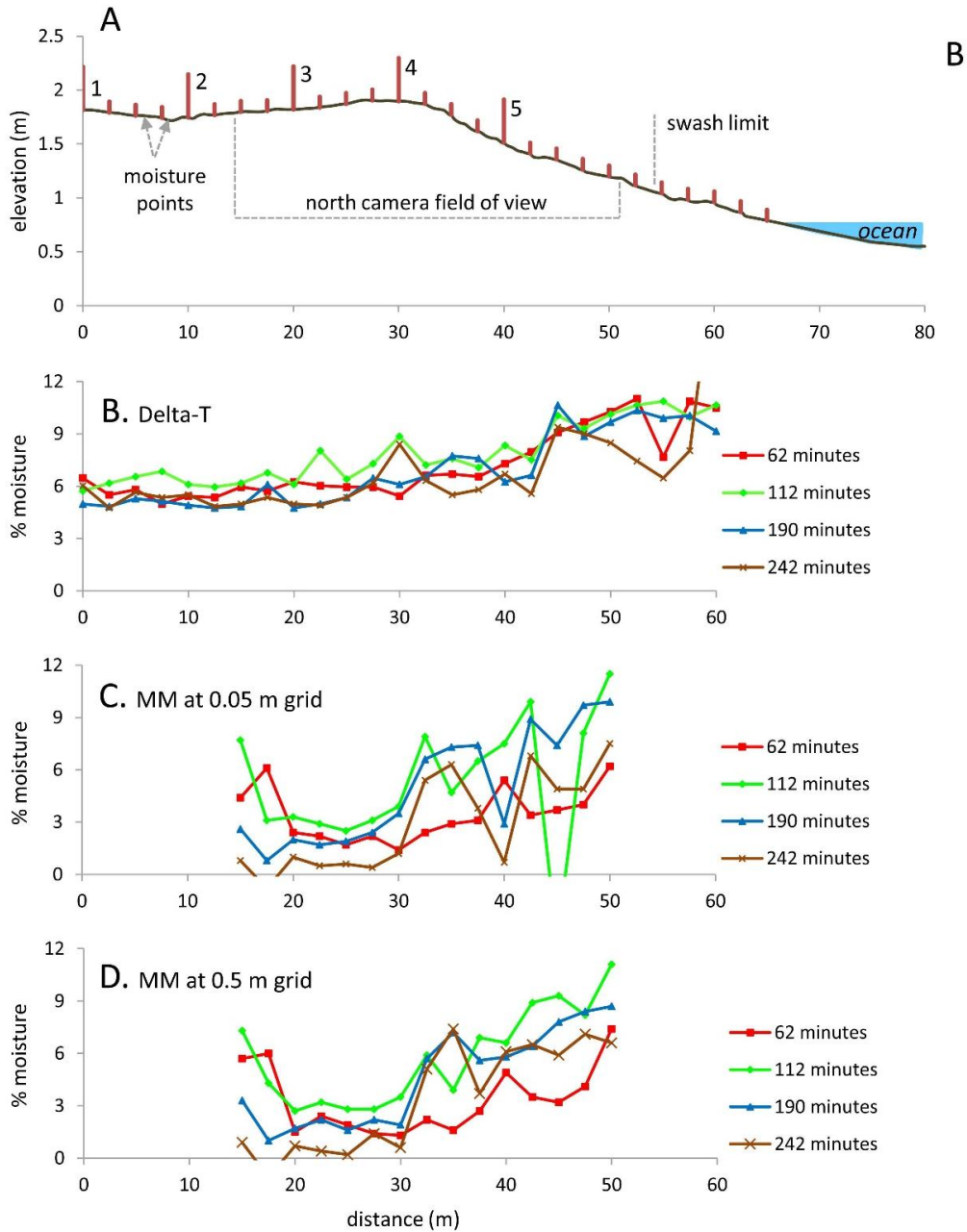


Figure 7: A) Beach profile along the instruments transect; B) Measurements of near surface moisture (upper 2 cm) taken at four times along the instrument profile using the Delta-T Theta Probe; C) Surface moisture at the same four times and locations (within the field of view of the camera) estimated from moisture maps at the original grid resolution of 0.05 m; D) Measurements of surface

moisture from moisture maps at a coarser resolution of 0.5 m.

626

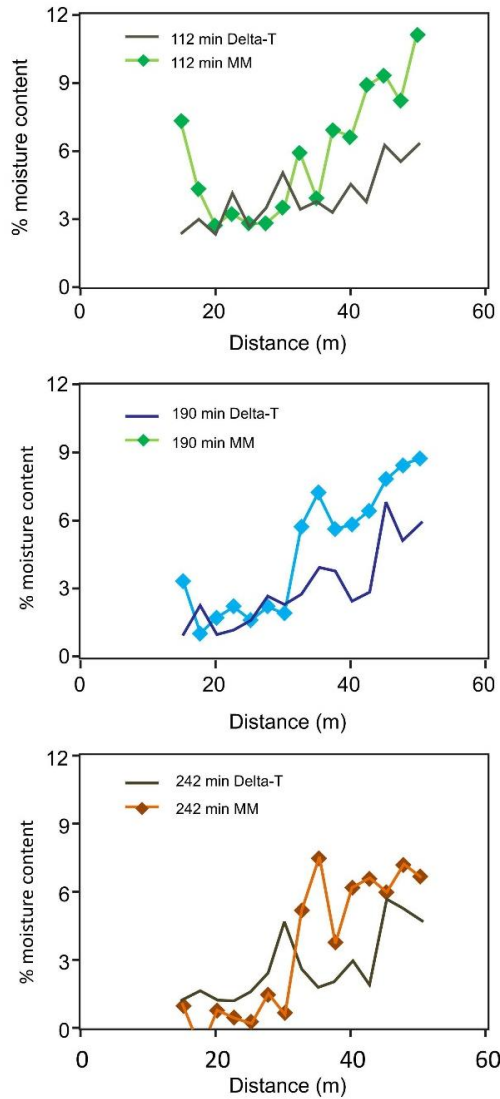


Figure 8: Plot of moisture values from the Delta-T Theta probe and moisture maps (MM) at 0.5 m grid resolution at three different time intervals. In general terms, the MM values show a larger variability of moisture values and sharper differences between the wettest and driest ends.

627

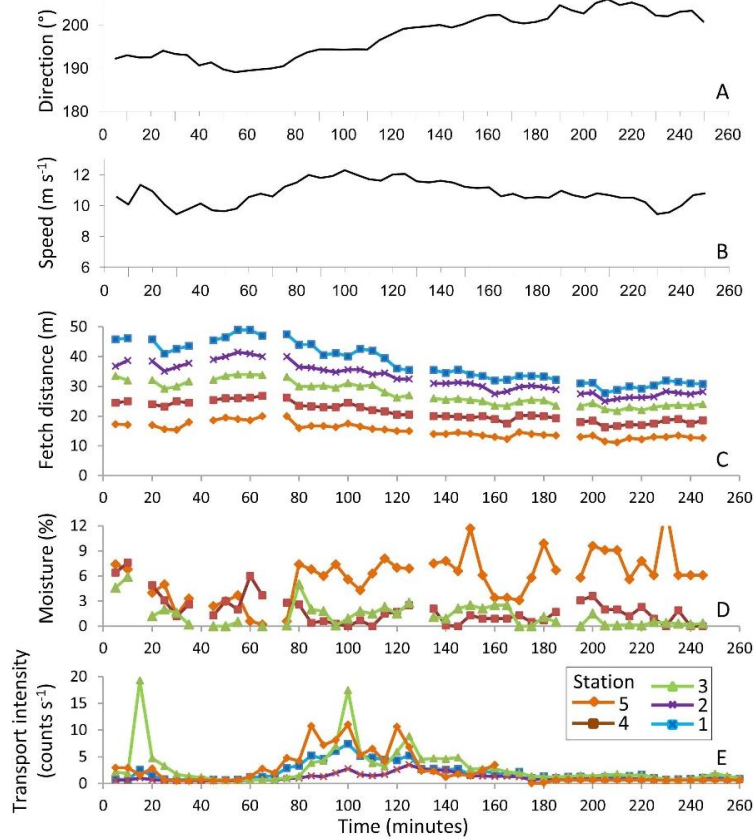


Figure 9: Five minute averages for incident wind direction (A) and wind speed (B) recorded at 3 m high over the beach surface at station 4, fetch distances (C), surface moisture content for stations 3-5 (within the field of view of the camera; D), and sediment transport intensity (E). Gaps in the data correspond to periods of time when no images were taken.



Figure 10: Photographs of the beach surface at the end of the transport event: A) close-up of station 4; B) ripples formed in the dry sand accumulation at station 2; C) view of station 4 looking landward showing the eroded and relatively damp surface with a transition to deposition towards station 3 in the background.